

Toward new proton exchange batteries based on ionic liquid electrolyte: metal hydride electrode / electrolyte coupling

N. Chaabene¹, J. Zhang¹, M. Turmine^{2,3}, E. Kurchavova^{2,3}, V. Vivier^{2,3}, F. Cuevas¹, M. Latroche^{†,1}, J. Monnier^{‡,1}

1: Univ. Paris Est Créteil, CNRS, ICMPE, UMR 7182, 2 rue Henri Dunant, 94320 Thiais, France

2: Sorbonne Université, CNRS, Laboratoire de Réactivité de Surface UMR 7197, 4 Place Jussieu, 75005, Paris, France

3: Sorbonne Université, CNRS, Laboratoire Interfaces et Systèmes Electrochimiques, UMR 8235, 4 Place Jussieu, 75005, Paris, France

Supplementary information

To confirm the structure of synthesized pyrrolidinium acetate ([Pyrr][Ac]), Attenuated Total Reflectance-Fourier Transform Infrared (ATR-FTIR) spectra of pyrrolidine (Pyrr), acetic acid (Ac.A), and [Pyrr][Ac] were recorded and compared (Fig. S1a).

Wide signals in the ranges 2500-2700 cm^{-1} and 2750-3100 cm^{-1} on the spectrum of Ac.A and Pyrr, respectively, are associated with C-H vibrations [1] confirming the presence of acetate and pyrrolidinium group on the spectrum of [Pyrr][Ac]. Furthermore, on the spectrum of [Pyrr][Ac], new absorption bands at 1394 and 1553 cm^{-1} were observed. These signals can be attributed to unprotonated form of COO^- [2], which confirms the proton transfer from the carboxylic group to the nitrogen of pyrrolidinium. On the spectrum of Ac.A (red), a wide signal in the range 2900-3200 cm^{-1} associated with O-H vibrations of -COOH [1], and its absent on [Pyrr][Ac] (blue) also confirm this hypothesis.

On the other hand, the appearance of absorbance peak near $\sim 1700 \text{ cm}^{-1}$ on the spectrum of Ac.A (red) and [Pyrr][Ac] (blue) which can be associated with C=O (stretch) [1] testifies a probable equilibrium between protonated and unprotonated forms of carboxylic group.

[†] We honour our very dear Michel Latroche who significantly contributed to this scientific project and suddenly passed away.

[‡] Corresponding author: monnier@icmpe.cnrs.fr

The appearance of peak at 3260 cm^{-1} on the spectrum of Pyrr corresponds to N-H vibration of pyrrolidine [1]. However, this peak is not observed on the spectrum of [Pyrr][Ac]. The phenomenon could be linked to the formation of pyrrolidinium cation (Pyrr^+) with a positive charge on the nitrogen, that can lead to the shift of the signal and can be superposed with other signals around 3000 cm^{-1} .

All aforementioned results and hypotheses are in a good agreement with ^1H and ^{13}C Nuclear Magnetic Resonance (NMR) spectra (Fig. S1b) [3].

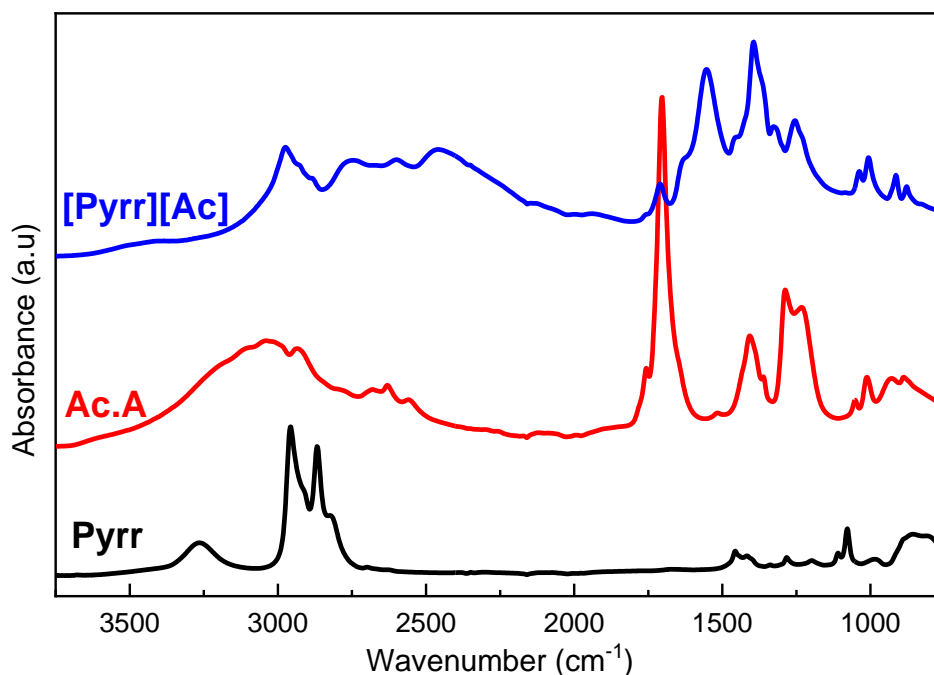


Figure S1a: ATR-FTIR spectra of Pyrr – black, Ac.A – red, [Pyrr][Ac] – blue.

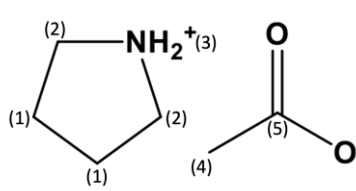
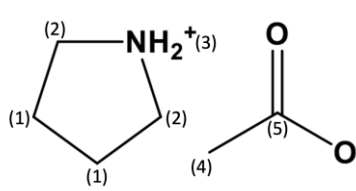
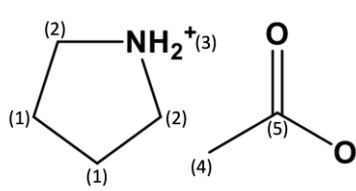
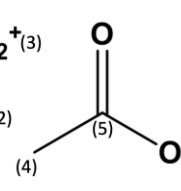
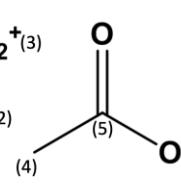
| Functional group | ^1H Chemical shift, ppm | ^{13}C Chemical shift, ppm |
|---|----------------------------------|-------------------------------------|
|  CH_2 (1) | 1.87 | 24.54 |
|  CH_2 (2) | 3.21 | 44.30 |
|  NH_2^+ (3) | 11.00 | - |
|  CH_3 (4) | 1.96 | 21.03 |
|  COO^- (5) | - | 168.66 |

Figure S1b: ^1H - and ^{13}C -NMR characteristics of [Pyrr][Ac].

The density ρ as a function of temperature for pure [Pyrr][F], [Pyrr][Ac], mixture of [Pyrr][Ac]/Ac.A or [Pyrr][Ac]/Pyrr, and a mix of [EMIM][Ac]/Ac.A are presented in Figure S2. All related data are gathered in Table S1. The density depends on the nature of the anion and the cation forming the IL. For the same cation (Pyrr⁺), when the acetate is replaced by the formate anion, the density decreases. It is noted that the [EMIM][Ac], which is an aprotic IL, mixed with Ac.A has the highest density.

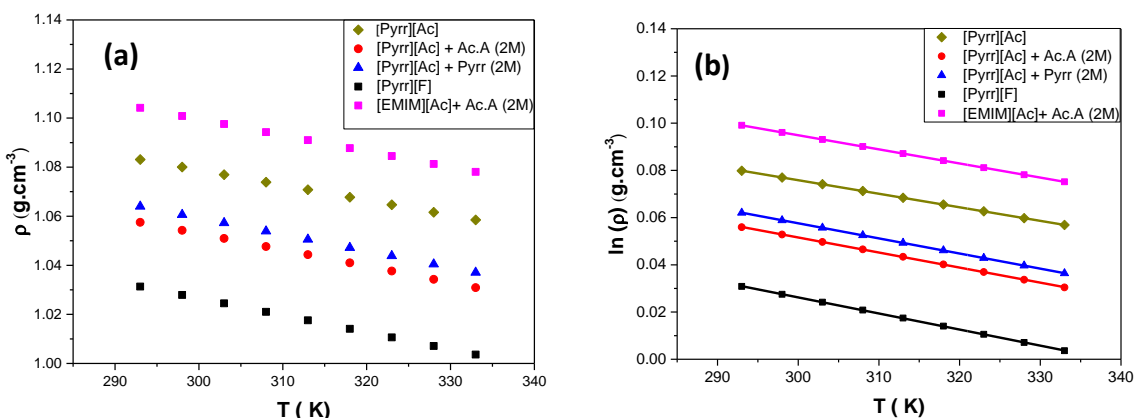


Figure S1 : Variations of (a) the density and (b) the logarithm of the density as a function of the temperature of the ionic liquids reported in this study.

Table S1: Density measurements as a function of temperature in the [20-60] °C range for [Pyrr][F], [Pyrr][Ac], [EMIM][Ac] and [Pyrr][Ac] mixed with acetic acid or pyrrolidinium. Three measurements have been performed, the magnitudes are presented in this table, the standard deviation is $\pm 0.00005 \text{ g.cm}^{-3}$.

| Temperature (°C) | [Pyrr][F] | [Pyrr][Ac] | [Pyrr][Ac] + Ac.A | [Pyrr][Ac] + Pyrr | [EMIM][Ac] + Ac.A |
|------------------|-----------|------------|-------------------|-------------------|-------------------|
| 60 | 1.05852 | 1.03089 | 1.03708 | 1.00361 | 1.07808 |
| 55 | 1.06159 | 1.03428 | 1.04045 | 1.00713 | 1.08129 |
| 50 | 1.06466 | 1.03765 | 1.04382 | 1.01063 | 1.08452 |
| 45 | 1.06774 | 1.04100 | 1.04718 | 1.01412 | 1.08776 |
| 40 | 1.07081 | 1.04434 | 1.05055 | 1.01759 | 1.09102 |
| 35 | 1.07388 | 1.04766 | 1.05391 | 1.02104 | 1.09429 |
| 30 | 1.07695 | 1.05096 | 1.05727 | 1.02448 | 1.09757 |
| 25 | 1.08003 | 1.05425 | 1.06064 | 1.02791 | 1.10086 |
| 20 | 1.08311 | 1.05753 | 1.06401 | 1.03133 | 1.10417 |

The density of ionic liquids and their mixtures with Ac.A or Pyrr decreases linearly when the temperature increases (Fig. S2a). Measurements of density as a function of temperature allow us

to determine the coefficient of thermal expansion, α , according to equation S1. This coefficient represents the relative increase in volume of a system as the temperature changes.

$$\alpha = -\frac{1}{\rho} \left(\frac{\partial \rho}{\partial T} \right) \quad (Eq. S1)$$

Thus, the logarithm of the density ($\ln \rho$) was plotted against the temperature. A linear dependence was obtained for the different media as shown on Figure S1.b. The slope value corresponds to the thermal expansion coefficient. Table S2 presents the thermal expansion coefficients for the ILs and their mixtures with Ac.A or Pyr. The protic IL [Pyr][F] has the lowest thermal expansion coefficient ($5.74 \cdot 10^{-4} \text{ K}^{-1}$). The thermal expansion coefficient slightly increases when formate was replaced by acetate anion and when acetic acid or pyrrolidine was added to the pure IL.

Table S2: Fitting parameters of room temperature experimental viscosity and conductivity of the studied ILs using Arrhenius equations where η_{∞} and σ_{∞} are the viscosity and conductivity at infinite temperature, E_{η} and E_{σ} are the activation energy of viscosity and conductivity, respectively. α is the thermal expansion coefficient.

| Medium | α ($/10^{-4} \text{ K}^{-1}$) | E_{η} ($\text{kJ} \cdot \text{mol}^{-1}$) | η_{∞} ($\text{mPa} \cdot \text{s}$) | E_{σ} ($\text{mS} \cdot \text{cm}^{-1}$) | σ_{∞} ($\text{mS} \cdot \text{cm}^{-1}$) |
|-----------------------|---|---|--|--|---|
| [Pyr][F] | 5.74 | 21.92 | 0.19 | 4.4233 | 219.37 |
| [Pyr][Ac] | 6.37 | 30.21 | 1.84 | 11.57904 | 877.79 |
| [Pyr][Ac] + Ac.A (2M) | 6.40 | 28.24 | 3.31 | 10.84951 | 733,61 |
| [Pyr][Ac] + Pyr (2M) | 6.80 | 27.34 | 3.31 | 9.02515 | 350.32 |
| [EMIM][Ac]+Ac.A (2M) | 5.97 | 31.51 | 1,633 | 15.85228 | 3541,42 |

Dynamic viscosity is the internal resistance of a fluid to shear a strain. This parameter impacts the transport of matter in the solution. Therefore, it significantly affects the diffusion of hydrogen in the environment. We systematically measured the dynamic viscosity η of the five studied media according to the temperature between 20 and 60°C with a step of 5°C (Figure S2 and Table S3). As expected, the viscosity decreases with the temperature. The comparison of viscosity values for [Pyr][Ac], pure or mixed with 2 M of Ac.A or Pyr evidences that the acid or the base enable to decrease the viscosity.

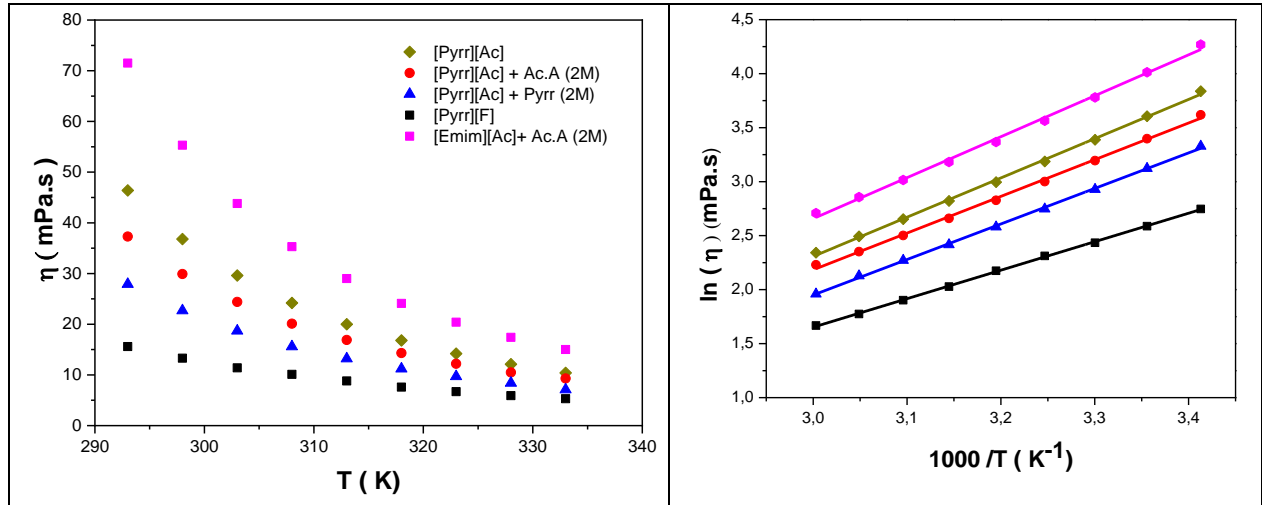


Figure S2 : Dynamic viscosity measurements as a function of temperature in the [20-60] °C range for [Pyrr][F], [Pyrr][Ac], [EMIM][Ac] and [Pyrr][Ac] mixed with Ac.A or Pyrr.

Table S3: Viscosity measurements as a function of temperature in the [20-60] °C range for [Pyrr][F], [Pyrr][Ac], [EMIM][Ac] and [Pyrr][Ac] mixed with Ac.A or Pyrr.

| Temperature (°C) | [Pyrr][F] | [Pyrr][Ac] | [Pyrr][Ac] + Ac.A | [Pyrr][Ac] + Pyrr | [EMIM][Ac] + Ac.A |
|------------------|-----------|------------|-------------------|-------------------|-------------------|
| 60 | 5.3 | 10.4 | 9.3 | 7.1 | 15.0 |
| 55 | 5.9 | 12.1 | 10.5 | 8.4 | 17.4 |
| 50 | 6.7 | 14.2 | 12.2 | 9.7 | 20.4 |
| 45 | 7.6 | 16.8 | 14.3 | 11.2 | 24.1 |
| 40 | 8.8 | 20.0 | 16.9 | 13.2 | 29.0 |
| 35 | 10.1 | 24.2 | 20.1 | 15.6 | 35.3 |
| 30 | 11.4 | 29.6 | 24.4 | 18.7 | 43.8 |
| 25 | 13.3 | 36.8 | 29.9 | 22.7 | 55.3 |
| 20 | 15.6 | 46.4 | 37.3 | 27.9 | 71.5 |

The temperature dependence of the viscosity values is most often fitted using an Arrhenius-like relationship, which expresses as:

$$\ln(\eta) = \ln \eta_{\infty} + \frac{E_{\eta}}{RT} \quad (\text{Eq. S2})$$

where E_{η} is the activation energy, η the viscosity, η_{∞} the pre-exponential factor and R the perfect gas constant. Eq. S2 can be applied to describe the temperature dependence of the viscosity in a narrow temperature range. For larger temperature range, semi-empirical approach the so-called Vogel-Tamman-Fulcher (VTF) relationship is commonly used to describe this temperature dependence (1). Table S2 gathers the activation energies, E_{η} , and the viscosities at infinite

temperature, η_{∞} , for the different medium. E_{η} is the energy barrier that must be overcome by the ions to move through the medium. E_{η} , increases and η_{∞} decreases slightly when the acetic acid was added.

Similarly, to the viscosity, variations in the conductivity (σ) of the five media over a temperature range from 20 to 60 °C are reported on Figure S3, with all the data reported in Table S4. As expected, the conductivity increases with the temperature due to increase of ion mobility and decrease of the viscosity.

As detailed in (15), the viscosity of the IL plays an important role in the variation in conductivity since the diffusion coefficient D_i of ion is linked to viscosity by the Stokes-Einstein equation (Eq S3) in which the ions are assumed to have a spherical, effective radius r_i shape.

$$D_i = \frac{k_b T}{6\pi r_i \eta} \quad (\text{Eq. S3})$$

With Boltzmann's constant k_b , T the temperature in K and η dynamic viscosity. The conductivity of the ion i , σ_i , can be expressed according to Nernst-Einstein's relationship:

$$\sigma_i = \frac{c_i z_i^2 F^2 D_i}{RT} \quad (\text{Eq. S4})$$

Where z_i stands for the valence of the charge carrier, c_i is the molar concentration and F the Faraday constant.

By combining the last two relations:

$$\sigma_i = \frac{c_i z_i^2 F^2}{6\pi N_a r_i \eta} \quad (\text{Eq. S5})$$

So, there is a link between viscosity and conductivity which states that an IL with a low viscosity will present a high conductivity, and reversibly an IL with higher viscosity will present lower conductivity. Fig. S4 shows that addition of acid or base increases the conductivity of the IL. All the IL-based media present conductivity higher than 1 mS.cm⁻¹, considered as the critical value for an IL to be used as an electrolyte.

Since conductivity is related to viscosity the variation of conductivity as a function of temperature also follows the law of Arrhenius (eq S6).

$$\ln(\sigma) = \ln(\sigma^\infty) + \frac{E_\sigma}{RT} \quad (\text{Eq. S6})$$

Table S4: conductivity measurements as a function of temperature in the [20-60] °C range for [Pyrr][F], [Pyrr][Ac], [EMIM][Ac], and [Pyrr][Ac] mixed with Ac.A or Pyrr. The standard deviation is $\pm 0.1 \text{ mS}\cdot\text{cm}^{-1}$.

| [Pyrr][F] | | [Pyrr][Ac] | | [Pyrr][Ac] + Ac.A. | | [Pyrr][Ac] + Pyrr | | [EMIM][Ac] + Ac.A. | |
|-----------|---------------|------------|---------------|--------------------|---------------|-------------------|---------------|--------------------|---------------|
| T | σ_{IL} | T | σ_{IL} | T | σ_{IL} | T | σ_{IL} | T | σ_{IL} |
| °C | mS/cm | °C | mS/cm | °C | mS/cm | °C | mS/cm | °C | mS/cm |
| 21.7 | 36.0 | 23.6 | 7.8 | 23.5 | 8.8 | 24.0 | 9.0 | 23.5 | 5.5 |
| 23.6 | 36.3 | 23.8 | 7.8 | 23.8 | 8.7 | 24.2 | 9.0 | 23.7 | 5.5 |
| 25.9 | 37.3 | 27.8 | 8.4 | 27.5 | 9.4 | 28.0 | 9.5 | 27.5 | 6.0 |
| 27.7 | 37.2 | 28.0 | 8.4 | 27.6 | 9.4 | 28.2 | 9.5 | 27.7 | 6.1 |
| 30.2 | 38.1 | 31.8 | 9.0 | 31.5 | 10.1 | 32.3 | 9.0 | 31.6 | 6.7 |
| 32.3 | 38.2 | 32.2 | 9.0 | 31.6 | 10.0 | 32.4 | 10.0 | 31.8 | 6.7 |
| 34.4 | 39.0 | 36.0 | 9.6 | 35.7 | 10.7 | 36.3 | 10.5 | 35.7 | 7.3 |
| 36.0 | 39.1 | 36.3 | 9.6 | 35.9 | 10.7 | 36.6 | 10.5 | 36.0 | 7.4 |
| 38.6 | 39.9 | 40.4 | 10.2 | 39.8 | 11.3 | 40.5 | 11.0 | 39.9 | 8.0 |
| 40.0 | 40.0 | 40.7 | 10.3 | 39.8 | 11.3 | 40.9 | 11.0 | 40.0 | 8.0 |
| 42.8 | 40.8 | 44.7 | 10.9 | 43.8 | 11.9 | 44.7 | 11.5 | 44.1 | 8.7 |
| 44.3 | 41.0 | 44.8 | 10.9 | 43.9 | 12.0 | 45.1 | 11.5 | 44.1 | 8.6 |
| 47.2 | 41.7 | 48.7 | 11.4 | 47.8 | 12.5 | 49.0 | 11.9 | 48.1 | 9.4 |
| 48.3 | 41.8 | 49.2 | 11.5 | 48.0 | 12.6 | 49.5 | 12.0 | 48.4 | 9.3 |
| 52.6 | 42.7 | 52.9 | 12.0 | 51.9 | 13.2 | 53.2 | 12.4 | 52.2 | 9.9 |
| 54.0 | 43.0 | 53.4 | 12.1 | 52.0 | 13.2 | 53.8 | 12.5 | 52.3 | 10.0 |
| 56.8 | 43.6 | 56.9 | 12.6 | 56.1 | 13.8 | 57.5 | 12.9 | 56.4 | 10.5 |
| 56.8 | 43.5 | 57.6 | 12.7 | 56.2 | 13.8 | 58.2 | 12.9 | 56.5 | 10.7 |

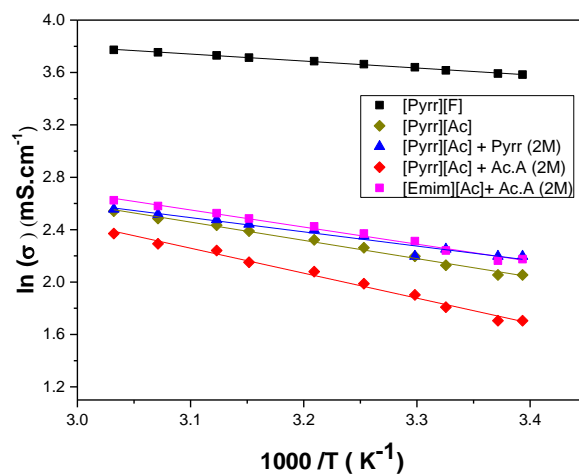


Figure S3 : Conductivity measurements as a function of temperature in the [20-60] °C range for [Pyrr][F], [Pyrr][Ac], [EMIM][Ac] and [Pyrr][Ac] mixed with Ac.A or Pyrr.

The hydroxymethylferrocene or ferrocenemethanol (FcMeOH), which is soluble in all studied ILs or mixtures, is used as a reference redox pair, to calibrate the different reference electrodes to $E^\circ(\text{FcMeOH})$ (Table S5). This electroactive species is commonly used as a probe-model molecule (2).

First, the electrochemical behavior of FcMeOH, in each medium was studied by cyclic voltammetry (CV) by varying the scan rate (Figure S4a). CVs clearly exhibit a quasi-reversible behavior, in which the ratio between the current density of the anodic peak j_{pa} and that of the cathodic peak j_{pc} is close to 1 also at high scan rates whereas the difference between the anodic and cathodic peak potentials are in agreement with the predicted values ($E_{pa} - E_{pc} \approx 60$ mV) for a mass-transfer controlled system. Current density peak (j_{pa}) varies linearly with the square root of the scan rate (Figure S4.b) showing that the mass transfer of FcMeOH in the investigated ILs is controlled by the diffusion of electroactive species (3).

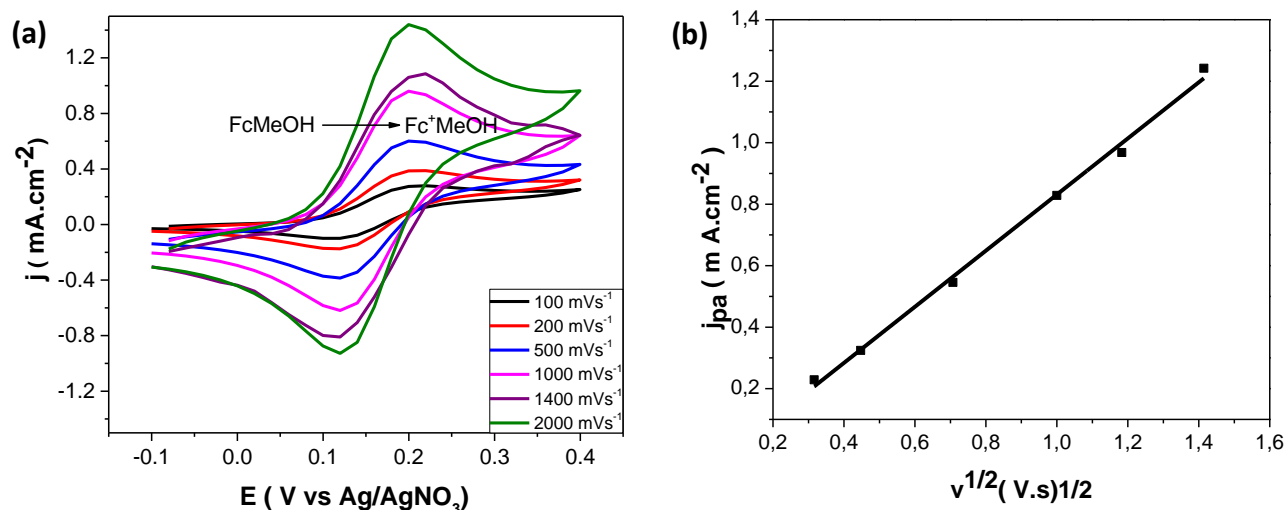


Figure S4 : (a) CV of a 5mM FcMeOH in [Pyrr][Ac] + Ac.A (2M) at different scan rates (from 100 to 2000 mV s⁻¹); (b) variation of the current density peak j_{pa} with the square root of the scan rate for the FcMeOH oxidation in [Pyrr][Ac] + Ac.A (2M). All these experiments were performed, at 25±0.1 °C, with a gold working electrode (200 μm in diameter).

For this scan rate domain, the diffusion coefficient of FcMeOH can thus be obtained from the slope of the current intensity curve as a function of square root of sweep rate by using Randles-Sevcik equation

$$i_p = 0.44nFA \left(\frac{nF}{RT} \right)^{\frac{1}{2}} CD^{\frac{1}{2}} \nu^{\frac{1}{2}} \quad (\text{eq. S7})$$

where i_p is the current of the peak, n the number of exchanged electron, A the electrode surface area (in cm^2), F the Faraday constant, D the diffusion coefficient (in $\text{cm}^2 \cdot \text{s}^{-1}$), C the concentration of the electroactive species in mol cm^{-3} , and ν the scan rate (in V s^{-1}).

The diffusion coefficients values of FcMeOH in different media are presented in Table S5. It should be noticed that the diffusion coefficients obtained in each medium are of the same order of magnitude. The diffusion coefficient of FcMeOH in [EMIM][Ac] is smaller than all other media. Indeed, as indicated in equation S3 the diffusion coefficient is inversely proportional to the viscosity of the media, shown in Table S5, the mixture of [EMIM][Ac] + Ac.A has the highest viscosity, which explains the less efficient mass transport corresponding to smallest value of the diffusion coefficient.

Table S5 : Values of the EW and standard potential of FcMeOH in ILs at 298K

| Electrolyte | EW (V) | $E^{\circ}(\text{FcMeOH})$ (V vs Ag/AgNO ₃) | η (mPa.s ⁻¹) | $D \cdot 10^{-7}$ (cm ² .s ⁻¹) |
|------------------------|--------|---|-------------------------------|---|
| KOH | 1.9 | INSOLUBLE | 5 | - |
| [Pyrr][F] | 2.0 | 0.14 | 13.3 | 4.2 |
| [Pyrr][Ac] | 2.2 | 0.16 | 36.8 | 3.3 |
| [Pyrr][Ac] + Pyrr (2M) | 2.4 | 0.15 | 22.7 | 5.1 |
| [Pyrr][Ac] + Ac.A (2M) | 2.3 | 0.16 | 9.9 | 4.6 |
| [EMIM][Ac] + Ac.A (2M) | 3.0 | 0.2 | 55.3 | 2.1 |

Linear Sweep Voltammetry (LSV) curves recorded on AB₅ electrode in [Pyrr][Ac] at the scan rate of 1 mV/s is shown on Fig. S6. It can be seen that electrolyte oxidation and reduction start at the potential around $E_a = 0.4$ V, and $E_c = -1.3$ V (vs. Ag/AgNO₃), respectively. Thereafter, within this potential range there is no electrolyte breakdown.

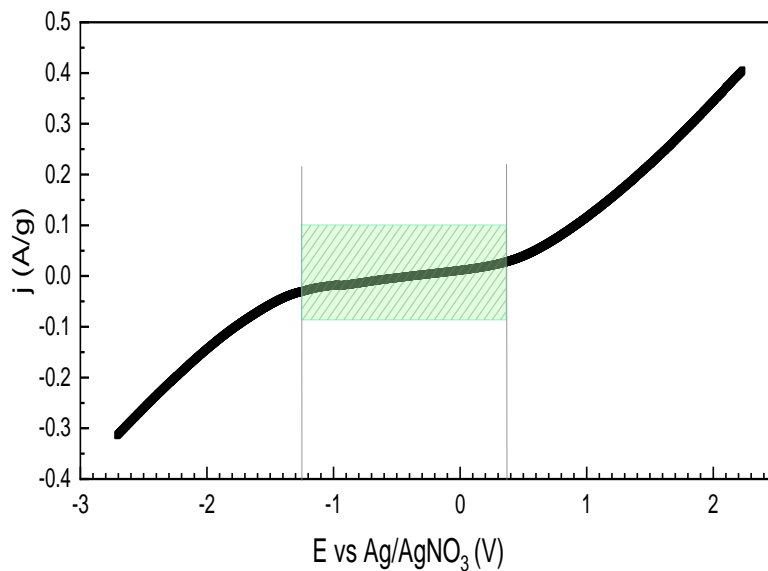


Figure S6. LSV curves recorded in [Pyrr][Ac] on AB_5 alloy at 25 ± 0.1 °C with a scan rate of 1 mV/s. The plateau within green box indicates the stability of electrolyte.

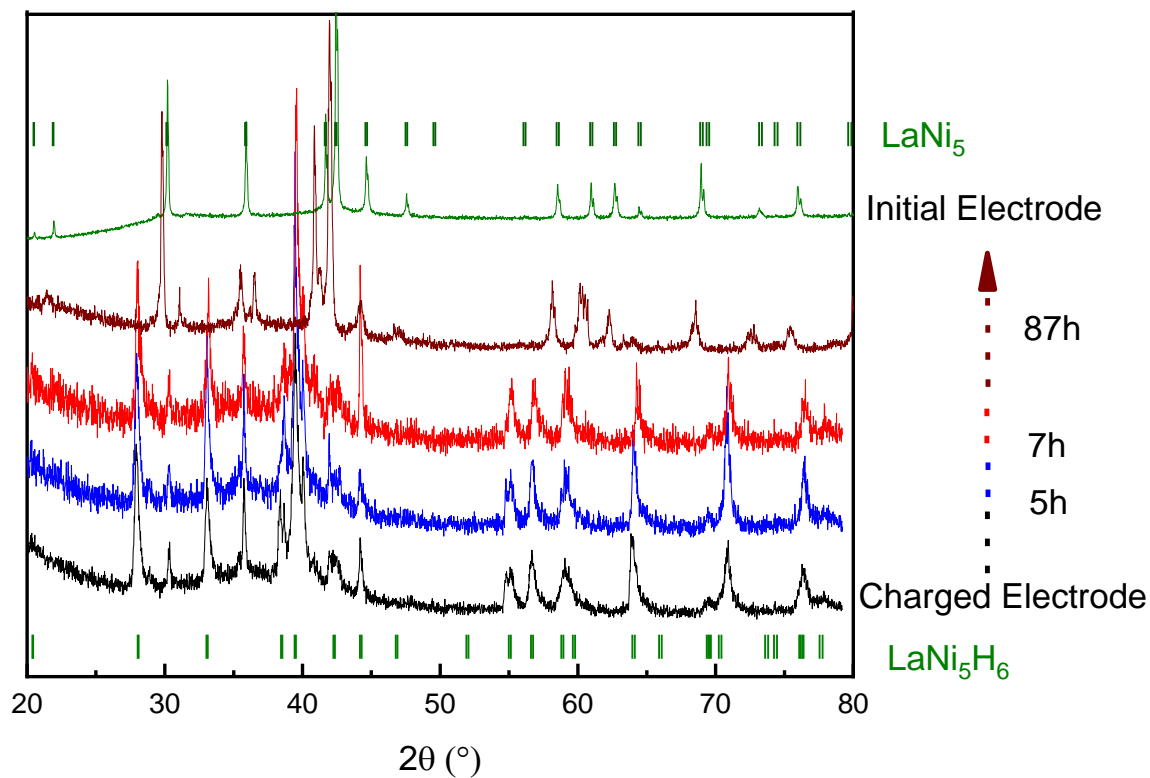


Figure S5: XRD patterns of the initial electrode, the electrode fully charged in [Pyrr][Ac] medium and time-evolution of XRD patterns this electrode during self-discharge under air. Bragg positions of $LaNi_5$ -type structure and $LaNi_5H_6$ -type hydride phase are indicated.

- [1] L.G. Wade, Jr., *Organic Chemistry*, 6th ed. Pearson Prentice Hall Inc., 2006.
- [2] R. I. Aravena and J. P. Hallett, "Protic ionic liquids based on fatty acids: A mixture of ionic and non-ionic molecules," *J Mol Liq*, vol. 373, Mar. 2023, doi: 10.1016/j.molliq.2023.121241.
- [3] M. Anouti, M. Caillon-Caravanier, Y. Dridi, H. Galiano, and D. Lemordant, "Synthesis and characterization of new pyrrolidinium based protic ionic liquids. Good and superionic liquids," *Journal of Physical Chemistry B*, vol. 112, no. 42, pp. 13335–13343, Oct. 2008, doi: 10.1021/jp805992b.